INTERNATIONAL JOURNAL FOR NUMERICAL METHODS IN ENGINEERING
Int. J. Numer. Meth. Engng 2004; **59**:389–408 (DOI: 10.1002/nme.883)

Numerical solution of the Helmholtz equation with high wavenumbers

Gang Bao[1,2], G. W. Wei[1,3,*,†] and Shan Zhao[1]

[1]*Department of Computational Science, National University of Singapore, Singapore 117543, Singapore*
[2]*Department of Mathematics, Jilin University, Changchun 130023, People's Republic of China*
[3]*Department of Electrical and Computer Engineering, Michigan State University, East Lansing, MI 48824, U.S.A.*

SUMMARY

This paper investigates the pollution effect, and explores the feasibility of a local spectral method, the discrete singular convolution (DSC) algorithm for solving the Helmholtz equation with high wavenumbers. Fourier analysis is employed to study the dispersive error of the DSC algorithm. Our analysis of dispersive errors indicates that the DSC algorithm yields a dispersion vanishing scheme. The dispersion analysis is further confirmed by the numerical results. For one- and higher-dimensional Helmholtz equations, the DSC algorithm is shown to be an essentially pollution-free scheme. Furthermore, for large-scale computation, the grid density of the DSC algorithm can be close to the optimal two grid points per wavelength. The present study reveals that the DSC algorithm is accurate and efficient for solving the Helmholtz equation with high wavenumbers. Copyright © 2003 John Wiley & Sons, Ltd.

KEY WORDS: Helmholtz equation; high wavenumber; pollution effect; discrete singular convolution; dispersion analysis

1. INTRODUCTION

It is well known that wave propagation problems for the Helmholtz equation involving high wavenumbers are notoriously difficult to solve numerically [1–4]. The very short wave problem governed by the Helmholtz equation has been recognized as one of remaining *unsolved* problems for modern numerical approaches [5]. Therefore, alternative new methods of approximation are urgently needed to attack the problem of very short waves [5].

*Correspondence to: G. W. Wei, Department of Electrical and Computer Engineering, Michigan State University, East Lansing, MI 48824, U.S.A.
†E-mail: wei@math.msu.edu

Contract/grant sponsor: National University of Singapore
Contract/grant sponsor: Michigan State University
Contract/grant sponsor: NSF Applied Mathematics Programs; contract/grant number: DMS 01-04001
Contract/grant sponsor: Office of Naval Research; contract/grant number: N000140210365

Received 8 July 2002
Revised 5 February 2003
Accepted 7 April 2003

Boundary-value problems (BVP) governed by the Helmholtz equation

$$-\Delta u - k^2 u = f \tag{1}$$

where f represents a harmonic source and k is the wavenumber, arise in a variety of important physical applications [6], especially in acoustic and electromagnetic wave propagation. The quality of the numerical solution of the Helmholtz equation depends significantly on the wavenumber k. Generally speaking, the solution at a high wavenumber k is highly oscillatory. Consequently, the discretization stepsize h of a numerical method has to be sufficiently refined to resolve the oscillations. A natural rule for such an adjustment is to force [1, 7, 8]

$$kh = \text{constant} \tag{2}$$

which implies the unchanged resolution, i.e. the same grid points (or elements) per wavelength used. However, it is known [1] that, for $kh = \text{constant}$, the errors of the finite element (FE) solutions deteriorate rapidly as the wavenumber k increases. This non-robust behaviour with respect to k is known as the 'pollution effect' [1–3, 8–14]. We refer to References [3, 9] for a formal definition of the pollution effect. Through a series of papers [1–3, 8–14], the pollution effect of the FE solutions to the Helmholtz equation has been carefully studied by Babuška and his collaborators. Sharp error estimates have been obtained under the small magnitude assumption of kh. In particular, it has been shown [1, 2] that the relative error of the h–p-version FE solutions in the H^1-seminorm satisfies

$$e_1 \leqslant C_1\theta + C_2 k\theta^2 \tag{3}$$

where $\theta = (kh/2p)^p$ and C_1, C_2 are constants independent of k, h. The first term in Equation (3) represents the error of the best approximation; while the second term is due to the pollution effect. The best approximation error is of the same order as the interpolation error on a discretized mesh and with bounded magnitude if $kh = \text{constant}$. For a high wavenumber k, the pollution term becomes the leading term in (3) and is responsible for the non-robustness behaviour with respect to k. On the other hand, it is clear from (3) that the pollution effect may be reduced by increasing p, i.e. the higher-order elements control the pollution well. The in-depth understanding of the pollution effect has facilitated some *a posteriori* estimates of the FE solutions [8, 12] and permitted adaptive control of the pollution [11]. Numerical investigations of the pollution effect in higher dimensions have been discussed in References [9, 14].

The pollution error is known to be directly related to the dispersion error [2, 8, 10, 13], i.e. the phase difference between the numerical and exact solutions. It is well known in numerical analysis that the quality of the numerical solution can be analysed through the dispersion analysis [8, 10, 13, 15]. From the dispersion analysis point of view, the numerical error of the FE solutions to the Helmholtz equation consists of two parts, the best approximation error and the dispersion error [10]. The best approximation is non-dispersive; while the dispersion is of the same order as the pollution error [2, 8, 10, 13]. The more the solution is dispersive, the stronger the pollution is. Hence, reduction of the pollution error is equivalent to the dispersion reduction of a numerical scheme [10].

In practice, the pollution effect of FE solutions for the Helmholtz equation limits reliable large scale wave computations [3]. For high wavenumber problems, the pollution effect can be avoided only when a very fine mesh is used. Consequently, for multi-dimensional large scale

problems that are hundreds of wavelengths in size, the FE approximation becomes prohibitively expensive. This provides the motivation for developing various modifications of the classical Galerkin FE method which reduce or eliminate the pollution error [3, 4, 7, 9, 16–21]. The success of these methods usually lies in the ability to include in the FE space *a priori* knowledge about the differential equation being solved, e.g. analytic knowledge about asymptotic solution, exact solution and singularity [4, 17–21]. As a consequence, the local basis of these FE methods will be non-polynomial shape functions. In one dimension, it has been shown that the pollution effect can be eliminated completely [3, 9]. However, it is proven [3] that the pollution effect is inevitable in multi-dimensions by using the FE method. Large scale problems which are especially difficult to solve in multi-dimensions call for alternative numerical approaches that either completely eliminate or substantially reduce the pollution error.

Recently, the discrete singular convolution (DSC) algorithm [22] has been developed as a potential numerical approach for solving various computational problems, including the Hilbert transform, processing of analytic signals and computational tomography. The mathematical foundation of the algorithm is the theory of distributions and the theory of wavelets [23]. The unified feature of the DSC formalism was discussed and it was demonstrated that computational methods of Galerkin, collocation, global, local and finite difference types can be derived from a single starting point in the framework of the DSC algorithm [24]. The DSC algorithm may be regarded as a local spectral method [25] and it has been used for the treatment of complex boundary conditions in structural analysis [26, 27] and applied to computational hydrodynamics [28]. Certain aspects of the convergence of the DSC algorithm have been discussed [25].

The main objective of the present work is to investigate the possible pollution effect of the DSC algorithm, and explore the feasibility of the DSC algorithm for solving the Helmholtz equation with high wavenumbers. In particular, we demonstrate that as a dispersion vanishing method, the DSC algorithm can be a pollution free scheme for solving the Helmholtz equation. The rest of this paper is organized as follows. A brief description of the DSC algorithm is presented in Section 2. The dispersive error of the DSC scheme is analysed and interpreted via the Fourier analysis in Section 3. The algorithm is illustrated through several numerical examples in Section 4. Finally, conclusions are drawn in Section 5.

2. THE DISCRETE SINGULAR CONVOLUTION

For the sake of clarity and integrity in presentation, a brief description of the DSC algorithm is given in this section. More detailed descriptions about various aspects of the DSC algorithm are available in References [22–24, 26].

2.1. Approximation of singular convolution

As a special class of mathematical transformations, singular convolutions appear in many science and engineering problems. In the context of distribution theory, a singular convolution can be defined by

$$F(t) = (T * \eta)(t) = \int_{-\infty}^{\infty} T(t - x)\eta(x)\,\mathrm{d}x \tag{4}$$

where T is a singular kernel and $\eta(t)$ is an element of the space of test functions. A singular kernel can be regarded as an element of the dual space of test functions and thus is a distribution. Depending on the form of the kernel T, the singular convolution (4) is the central issue for a wide range of science and engineering problems [22]. For data (surface) interpolation and solving partial differential equations (PDEs), singular kernels of delta type are useful

$$T(x) = \delta^{(n)}(x), \quad (n = 0, 1, 2, \ldots) \tag{5}$$

where $\delta(x)$ is the delta distribution. The singular kernel, $T(x) = \delta(x)$, is of particular importance for the interpolation of surfaces and curves. Higher-order kernels, $T(x) = \delta^{(n)}(x)$, $(n = 1, 2, \ldots)$ are essential for numerically solving PDEs and for image processing, noise estimation, etc. However, since these kernels are singular, they cannot be directly digitized in computers. Hence, the singular convolution, (4), is of little numerical merit. To avoid the difficulty of using singular expressions directly in computer, we construct sequences of approximations (T_α) to the distribution T [22]

$$\lim_{\alpha \to \alpha_0} T_\alpha(x) \to T(x) \tag{6}$$

where α_0 is a generalized limit. Obviously, in the case of $T(x) = \delta(x)$, each element in the sequence, $T_\alpha(x)$, is a delta sequence kernel. Note that one retains the delta distribution at the limit of a delta sequence kernel. In the previous numerical studies of the Helmholtz equation with high wavenumbers, similar idea has also been discussed in the partition of the unity method by Babuška and Melenk [17], and the approximation properties of a delta sequence kernel (or generally approximate delta function) were highlighted. The use of approximate delta functions as a tool in mathematical analysis was also mentioned in Reference [17].

With a sufficiently smooth approximation, it is useful to consider a *discrete singular convolution* (DSC) [22]

$$F_\alpha(t) = \sum_k T_\alpha(t - x_k) f(x_k) \tag{7}$$

where $F_\alpha(t)$ is an approximation to $F(t)$ and $\{x_k\}$ is an appropriate set of discrete points on which the DSC (7) is well defined. Note that, the original test function $\eta(x)$ has been replaced by a common function $f(x)$. The mathematical property or requirement of $f(x)$ is determined by the approximate kernel T_α.

2.2. DSC trial functions

There exist a variety of sequence kernels of delta type and these kernels can be classified as either positive type or Dirichlet type [24, 26]. For simplicity, only one important delta sequence kernel of Dirichlet type, Shannon's delta kernel, is discussed here. Shannon's delta kernel is given by the following (inverse) Fourier transform of the characteristic function, $\chi_{[-\alpha, \alpha]}$,

$$\delta_\alpha(x) = \frac{1}{2\pi} \int_{-\infty}^{\infty} \chi_{[-\alpha, \alpha]} e^{-i\xi x} \, d\xi = \frac{\sin(\alpha x)}{\pi x} \tag{8}$$

By definition, it recovers the delta distribution at the limit

$$\lim_{\alpha \to \infty} \int \frac{\sin \alpha(x - y)}{\pi(x - y)} \eta(y) \, dy = \eta(x) \tag{9}$$

For the purpose of digital computations, it is necessary to discretize delta kernels. To this end, we examine a sampling basis given by Shannon's delta kernel

$$S_k(x) = \frac{\sin \alpha(x - x_k)}{\pi(x - x_k)} \tag{10}$$

Such a sampling basis is obviously interpolative

$$S_k(x_l) = \delta_{k,l} \tag{11}$$

where $\delta_{k,l}$ is the Kronecker delta function. Computationally, being interpolative is desirable for numerical accuracy and simplicity. In fact, this sampling basis is also an element of the Paley Wiener reproducing kernel Hilbert space. It provides a discrete representation of every (continuous) function in B_π^2, that is

$$f(x) = \sum_{k \in Z} f(x_k) S_k(x), \quad \forall f \in B_\pi^2 \tag{12}$$

This is Shannon's sampling theorem and it means that one can recover a continuous bandlimited L^2 function from a set of discrete values. Shannon's sampling theorem had a great impact on information theory, signal and image processing because the Fourier transform of Shannon's delta kernel is an ideal low-pass filter. For numerical computations, Equation (12) can never be realized because it requires infinitely many sampling points. A truncation is required in practical computations. Unfortunately, Shannon's delta kernel decays slowly and leads to substantial truncation errors.

According to the theory of distributions, the smoothness, regularity and localization of a tempered distribution can be improved by regularization with a function of the Schwartz class. We apply this principle to regularize approximate convolution kernels [22]

$$\delta_{\alpha,\sigma}(x) = \delta_\alpha(x) R_\sigma(x), \quad (\sigma > 0) \tag{13}$$

where R_σ is a *regularizer* which has properties

$$\lim_{\sigma \to \infty} R_\sigma(x) = 1 \quad \text{and} \quad R_\sigma(0) = 1 \tag{14}$$

Various delta regularizers can be used for numerical computations. A good example is the Gaussian $R_\sigma(x) = \exp[-x^2/2\sigma^2]$ [22], where σ determines the width of the Gaussian envelop and is commonly varied in association with the grid spacing, i.e. $\sigma = rh$, where r is a constant. The regularized Shannon's delta kernel on an arbitrary grid is thus given by [22],

$$\delta_{h,r}(x - x_k) = \frac{\sin[(\pi/h)(x - x_k)]}{(\pi/h)(x - x_k)} \exp\left[-\frac{(x - x_k)^2}{2(rh)^2}\right] \tag{15}$$

Expression (15) is sampled at the Nyquist frequency, π/h, which yields the highest accuracy and efficiency.

Immediate benefit from the regularized Shannon's kernel function (15) is that its Fourier transform is now infinitely differentiable. Qualitatively, Shannon's kernel has a long tail in the co-ordinate representation which is proportional to $1/x$, whereas, the regularized kernels decay exponentially fast. In the Fourier domain, (untruncated) Shannon's kernel is an ideal low-pass filter, which is discontinuous at frequency $\omega = \pi/h$. What makes Shannon's kernel

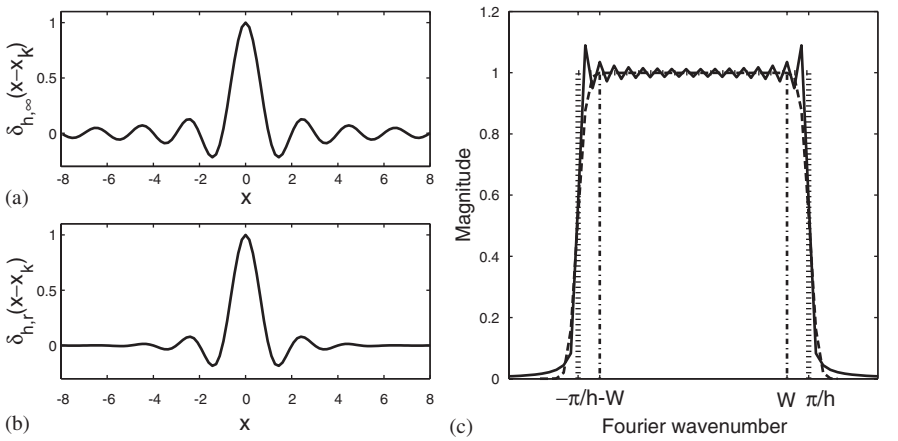

Figure 1. Plots of regularized and normal Shannon's delta kernels and their frequency response: (a) Shannon's delta kernel; (b) regularized Shannon's delta kernel; and (c) frequency response of two kernels given by discrete Fourier analysis. In (c), dot: exact frequency response determined by the choice of a grid spacing h; solid line: truncated Shannon's delta kernel; dashed line: regularized Shannon's delta kernel; dash-dotted lines: the positions of the bandlimit within which the regularized Shannon's kernel has negligible truncation error.

computationally unfavourable is the truncation error. The truncated Shannon's kernel oscillates dramatically and diverses from the exact frequency response (i.e. the ideal low-pass filter), see Figure 1. In contrast, the regularized Shannon's kernels is free of oscillation and is almost exact for the frequency within a bandlimit W. Therefore, the truncation error is dramatically reduced by the use of the delta regularizer in practical numerical computations. This has been rigorously proved recently [25].

Theorem

For a bandlimited L^2 function f whose spectrum distribution is confined to the wavenumber W, assume that the frequency supported by the grid spacing π/h be $\pi/h > W$ and $M > |x|/h$. Then the computational error, i.e. the error within the Nyquist frequency range $|\omega| < \pi/h$ can be estimated as

$$\left| f(x) - \sum_{|k| \leqslant M} f(x_k)\delta_{h,r}(x - x_k) \right|$$

$$\leqslant C(rh)^{-1/2} W^{1/2} \frac{\exp(-r^2h^2(\pi/h - W)^2/2)}{\left(\sqrt{2} + rh(\pi/h - W)\right)(1 + rh(\pi/h - W))^{1/2}}$$

$$+ C \frac{rh\rho_{h,2}(f, M)\exp(-(Mh - |x|)^2/(2r^2h^2))}{\sqrt{Mh - |x|}(rh + Mh - |x|)} \tag{16}$$

where the constants C are independent of h, r, and M, and $\rho_{h,2}(f, M)$ is defined as

$$\rho_{h,2}(f, M) = \left(h \sum_{|k| \geqslant M} |f(x_k)|^2 \right)^{1/2} \tag{17}$$

The proof of the theorem is given in Reference [25] and is beyond the scope of the present paper. Essentially, this theorem states that for bandlimited L^2 functions, the aliasing error, i.e. the first term on the right-hand side of (16), of the regularized Shannon's sampling expansion is exponentially small as long as the Nyquist frequency π/h is chosen greater than the bandlimit W. Moreover, the truncation error, the second term on the right-hand side of (16), decays exponentially with respect to the increase in sampling points M. In other words, the DSC algorithm with the regularized Shannon's kernel can also achieve spectral accuracy of global methods. As the DSC algorithm is a local method, we call it a local spectral method.

2.3. Numerical implementation

Without the loss of generality, we consider a generic time-independent PDE of the form

$$\mathscr{L}u + F(u) = \sum_n d_n(x) \frac{\partial^n u}{\partial x^n} + F(u) = 0 \tag{18}$$

where $F(u)$ is a known source term, $d_n(x)$ are known coefficients and $\mathscr{L}$ is a linear differential operator. In the DSC algorithm, we approximate the function and its nth order derivative at point x by

$$f^{(n)}(x) \approx \sum_{k=-M}^{M} \delta_{h,r}^{(n)}(x - x_k) f(x_k) \quad (n = 0, 1, 2, \ldots) \tag{19}$$

where $2M + 1$ is the computational bandwidth and $\{x_k\}$ are centred around x. For a given $\delta_{h,r}(x - x_k)$, the higher order derivative terms can be given by means of *analytical* differentiation $\delta_{h,r}^{(n)}(x - x_k) = [(\mathrm{d}/\mathrm{d}x)^n \delta_{h,r}(x - x_k)]$. Owing to the approximation (19), it is simple to use the collocation scheme, in which an operator will be typically discretized on a grid of the co-ordinate representation. Therefore, a DSC discrete form of the genetic equation can be expressed as

$$\sum_n d_n(x_m) \sum_{k=m-M}^{m+M} \delta_{h,r}^{(n)}(x_m - x_k) u_k + F(u(x_m)) = 0 \tag{20}$$

Extensions to higher dimensions can be realized by tensor products.

3. DISPERSION ERROR ANALYSIS

We present the Fourier analysis of the dispersive error of the DSC algorithm in this section. For the Helmholtz equation, dispersive error analysis of the FE solution has been carried out by several authors [10, 13, 29] and applied to improve the quality of numerical algorithms [3, 7, 9, 16]. In general, discrete Fourier analysis is capable of revealing the Fourier resolution of an interpolation (differentiation) scheme applied to a class of bandlimited and periodic

functions [15]. Thus, one can easily calculate the dissipative and dispersive errors of a given scheme via such an analysis.

In the following, we analyse the Fourier resolution associated with the DSC algorithm for solving the one-dimensional homogeneous Helmholtz equation

$$\frac{\partial^2 u}{\partial x^2} + k^2 u = 0 \tag{21}$$

The analytical solution of (21) is a plane wave of the form

$$u(x) = A\mathrm{e}^{\pm \mathrm{i}kx} \tag{22}$$

with a constant amplitude $|u| = A$. The DSC approximation to Equation (21) is given by

$$\sum_{l=-M}^{M} \delta^{(2)}_{h,\sigma}(x_j - x_{j+l}) u_h(x_{j+l}) + k^2 u_h(x_j) = 0 \tag{23}$$

Note that Equation (23) is an interior stencil which does not take into account of boundary conditions. Thus the present analysis holds independent of boundary conditions [10]. An exponential solution to (23) is assumed to have the form: $u_h(x_j) = \mathrm{e}^{\mathrm{i}k^* x_j}$, where k^* is a modified wavenumber. By substituting this plane wave solution into (23) and noting that $x_{j+l} = x_j + lh$, we obtain

$$\sum_{l=-M}^{M} \delta^{(2)}_{h,\sigma}(x_j - (x_j + lh))\mathrm{e}^{\mathrm{i}k^*(x_j+lh)} + k^2 \mathrm{e}^{\mathrm{i}k^* x_j} = 0 \tag{24}$$

Removing the common term $\mathrm{e}^{\mathrm{i}k^* x_j}$ gives

$$\sum_{l=-M}^{M} \delta^{(2)}_{h,\sigma}(-lh)\mathrm{e}^{\mathrm{i}lk^* h} + k^2 = 0 \tag{25}$$

Following Deraemaeker *et al.* [13], for $M = 1$, the above equation can be rewritten as

$$2\delta^{(2)}_{h,\sigma}(h)\cos(k^* h) + \delta^{(2)}_{h,\sigma}(0) + k^2 = 0 \tag{26}$$

Thus, the modified wavenumber of the numerical solution is given by

$$k^* = \pm \frac{1}{h} \arccos\left(\frac{-k^2 - \delta^{(2)}_{h,\sigma}(0)}{2\delta^{(2)}_{h,\sigma}(h)}\right), \quad kh \leqslant \sqrt{12} \tag{27}$$

Since the DSC approximation to the second-order derivative operator is symmetric, it produces no amplitude error. In general, for arbitrary M, we have

$$\sum_{l=1}^{M} 2\delta^{(2)}_{h,\sigma}(lh)\cos(lk^* h) + \delta^{(2)}_{h,\sigma}(0) + k^2 = 0 \tag{28}$$

However, the analytical form of k^* is difficult to derive from (28).

Alternatively, the dispersion error can be analysed by means of a Fourier transform from the physical space to the frequency space

$$\mathscr{F}[u(x)] = \frac{1}{2\pi}\int_{-\infty}^{\infty} u(x)\mathrm{e}^{\mathrm{i}kx}\,\mathrm{d}x \tag{29}$$

The Fourier transform of the second-order derivative gives

$$\mathscr{F}\left[\frac{\partial^2 u}{\partial x^2}\right] = (\mathrm{i}k)^2\mathscr{F}[u(x)] \tag{30}$$

In the DSC algorithm, the derivatives are approximated by means of discrete convolution (19). In fact, by the convolution theorem, the corresponding Fourier coefficients of the derivatives satisfy

$$\mathscr{F}[\{\delta^{(2)}_{h,\sigma}(x)\}_M * u(x)] = \mathscr{F}[\{\delta^{(2)}_{h,\sigma}(x)\}_M]\cdot\mathscr{F}[u(x)] \tag{31}$$

where $*$ denotes the convolution. It follows that the modified wavenumber satisfies

$$(\mathrm{i}k^*)^2 = \mathscr{F}[\{\delta^{(2)}_{h,\sigma}(x)\}_M] \tag{32}$$

For convenience, we introduce the scaled wavenumbers $\omega^* = hk^*$ and $\omega = hk$, and a scaled co-ordinate $s = x/h$. We then have

$$(\omega^*)^2 = (hk^*)^2 = -\mathscr{F}[\{\delta^{(2)}_{1,\sigma}(s)\}_M] \tag{33}$$

Therefore, the dispersive error of the DSC algorithm can be measured by the closeness of $(\omega^*)^2$ to ω^2 within the domain of the wavenumber $\omega \in [-\pi, \pi]$. It is noted that at the ends of the domain, the Nyquist frequency π/h, which is the maximum wavenumber that could be distinguished by the discretization with the mesh size h, is reached. Any wavenumber whose absolute value is greater than the Nyquist frequency will be misinterpreted and contributes to the aliasing error.

The dispersive error of the DSC scheme is illustrated in Figure 2, where the discrete Fourier transform is used as a tool for calculating $(\omega^*)^2$. It is evident from Figure 2 that the DSC approximation stays close to the exact differentiation until a very high wavenumber. Several modified wavenumbers that are associated with different DSC parameters are depicted in Figure 2. These plots actually provide intuitive means for comparing different DSC kernels and for optimizing DSC parameters. It is clear that as M increases, the dispersive error decreases. For a fixed M, the dispersive errors of the DSC kernels can be controlled by adjusting $r = \sigma/h$. It appears from Figure 2(a) that the modified wavenumber $(\omega^*)^2$ gives a better approximation to the wavenumber ω^2, especially in the high wavenumber region, when a large r value is used. However, as also indicated in Figure 2(b), when r is too large, the dispersive error for low wavenumber becomes relatively large. Therefore, for a given grid density and fixed M, there exists a theoretically optimized r at which the global dispersive error is minimized.

For practical applications, however, it is actually not necessary to find the theoretically optimized r. Instead, an approximately optimized value of r can be easily chosen based on discrete Fourier analysis and is also capable of providing similarly accurate results. Assume

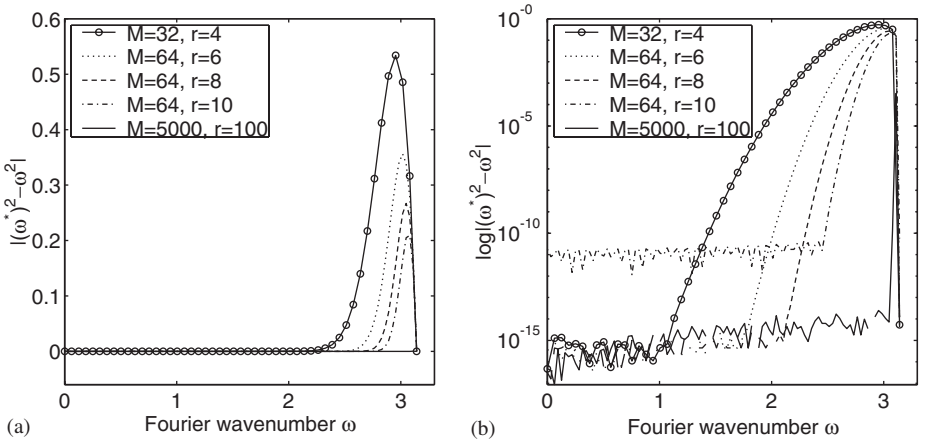

Figure 2. Dispersion errors: (a) the difference between the modified wavenumber $(\omega^*)^2$ and the wavenumber ω^2; and (b) the difference in the log scale.

the grid density (GD) is given as γ points per wavelength (PPW), then there exists a critical wavenumber ω_c,

$$\omega_c = 2\pi/\gamma \tag{34}$$

which represents the highest Fourier resolution that can be distinguished based on the given grid density. Thus, the approximation error introduced by the numerical scheme can be measured by the difference between ω^2 and $(\omega^*)^2$ within the interval $[0, \omega_c]$. Consequently, the effective dispersive error of the DSC algorithm may be characterized by $|\omega^2 - (\omega^*)^2| I_{\{0 \leqslant \omega \leqslant \omega_c\}}$, where I is an indicator function. By using such a criterion, for a fixed M, the approximately optimal r can be chosen as the one producing the smallest effective dispersive error through a few comparisons among different r values. For example, for GD = 3 PPW and $M = 64$ ($\omega_c = 2\pi/3$), in terms of the effective dispersive error, $r = 4$ is clearly the optimal one among several other r values in Figure 2. The corresponding dispersive error of the DSC algorithm is of machine limit. It should be noted that this simple method for selecting r though appears *ad hoc*, nevertheless, is quite general and robust. This is because that the choice of r depends only on GD and M, and is independent of the problem being studied. In fact, it is possible to tabulate all frequently used parameter combinations once for future use. Furthermore, the choice of the optimal value r may actually be chosen from a range without sacrificing the quality of the results. The robustness of the selection is demonstrated in the next section.

It is well known that pseudospectral methods can provide the highly accurate (exact) derivative approximation by using the GD of 2 PPW. Amazingly, when M is sufficiently large and r is appropriately chosen, the dispersion error of the DSC algorithm becomes negligible over nearly all possible ω. For example, the dispersive error of the DSC kernel with $M = 5000$ and $r = 100$ is as small as 10^{-14}, except when ω almost reaches π, see Figure 2. This finding is consistent with the previous studies [25] that the DSC algorithm can achieve the spectral accuracy of the Fourier spectral method. Since the reduction of the dispersion error is equivalent to the reduction of the pollution error [10], it is of great interest to study whether the pollution effect is presented for a dispersion vanishing algorithm.

4. NUMERICAL STUDIES

In this section, we test the numerical resolution and explore the ability of the DSC algorithm for solving the Helmholtz equation with high wavenumbers. In particular, it is interesting to test whether the pollution effect of the FE solutions occurs in the DSC solutions. For this purpose, a model problem governed by the one-dimensional Helmholtz equation is considered first [1, 2, 7]

$$\begin{gathered} -\frac{\partial^2 u}{\partial x^2} - k^2 u(x) = f(x) \\ u(0) = 0 \\ u'(1) - \mathrm{i}ku(1) = 0 \end{gathered} \tag{35}$$

Here, the computation domain is $\Omega = (0, 1)$. The mixed boundary condition at $x = 1$ is the Robin boundary condition which in the one-dimensional case is equivalent to the Sommerfeld radiation condition [7]. By using a constant forcing $f \equiv 1$, the exact solution of the BVP (35) reads

$$u(x) = \frac{1}{k^2}((1 - \cos(kx) - \sin(k)\sin(kx)) + \mathrm{i}(\cos(k) - 1)\sin(kx)) \tag{36}$$

To discretize the BVP (35), a uniform mesh with grid number N is used, thus the grid density is $\gamma = 2(N-1)\pi/k$ PPW. Consequently, $\omega_c = k/(N-1)$. The numerical relative error is measured in the H^1-seminorm defined by [1, 2]

$$e_1 := \frac{|u - u_h|_1}{|u|_1} \tag{37}$$

where u_h is the numerical approximation to the solution u, $|u|_1 = \|\mathrm{d}u/\mathrm{d}x\|$, and $\|u\|^2 = \int_\Omega u(x)\,\bar{u}(x)\,\mathrm{d}x$.

In the present study, following Babuška *et al.* [9], incorporation of the boundary conditions is considered separately from numerical discretization. In practice, a differentiation kernel in the DSC algorithm is typically applied in a translation invariant manner on the grid [22], which is similar to the interior stencil form (23) used in dispersion analysis. Hence, certain fictitious values located outside of the finite computational domain have to be obtained by using boundary conditions. The reader is referred to Reference [22] for additional discussions about the boundary issues of the DSC algorithm. For the present model problem, the discretization of the boundary conditions can be made analogous to that of a finite difference scheme [9, 30], due to the fact that the DSC algorithm may be degraded to the standard finite difference scheme [24]. The boundary discretizations may also be modelled via other suitable non-reflecting boundary conditions [31]. However, it is unclear how the modelling of the boundary conditions affects the results of dispersion analysis of the DSC algorithm, since the interior stencil is imposed on the infinite interval in the analysis [10]. Moreover, if the interior stencils lead to a pollution, then the effect cannot be eliminated by any modelling of the boundary condition [3, 9]. Therefore, if one attempts to focus only on the pollution effect introduced by the interior stencil, then certain appropriate modelling of the boundary conditions has to be employed. For example, based on a similar consideration, an optimal modelling of the boundary condition was used in

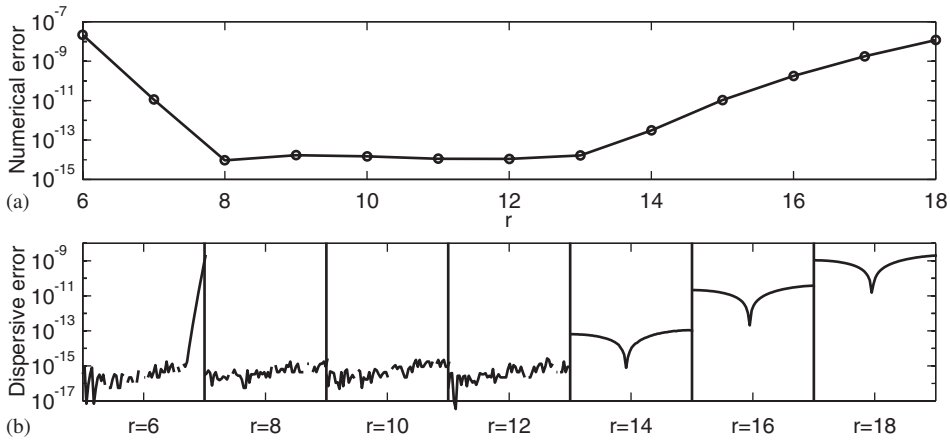

Figure 3. Discretization errors with different r: (a) the numerically tested H^1-seminorm relative errors; and (b) the dispersive errors of the DSC algorithm with $r = 6, 8, \ldots, 18$, within $0 \leqslant \omega \leqslant \omega_c$, where $\omega_c = 2\pi/\mathrm{GD} \approx 2.07$.

Reference [9]. In this paper, the pollution effect induced by the dispersion vanishing scheme is studied under a perfect boundary modelling, i.e. the fictitious values are adopted from the exact solution.

4.1. Numerical resolution of the DSC algorithm

In this subsection, we validate the findings of the Fourier error analysis of the DSC algorithm through numerical studies. In particular, we study the error behaviour by changing the DSC bandwidth M and parameter r. Consider a problem of the size: $N = 101$ and $k = 66\pi$. This problem is challenging to the conventional numerical schemes since the GD is about 3 PPW.

First, the accuracy change by varying ratio r is studied for a fixed $M = 100$. The relative errors in the H^1-seminorm and corresponding dispersive errors are shown in Figure 3. It is clear from Figure 3 that the DSC algorithm can provide an extremely high accuracy, even with GD as low as 3 PPW. Furthermore, the error of numerical results has an identical changing pattern as the dispersive error within $0 \leqslant \omega \leqslant \omega_c$, except for a little bit higher amplitude, which is due to relative measurement in numerical error. This indicates that numerical results are in excellent agreement with the dispersive error analysis. It should be emphasized that although the optimized r is theoretically unique for given M, in practice, an optimized r may be arbitrarily chosen from a range, e.g. $r \in [8, 13]$ in this example. The DSC algorithm with any $r \in [8, 13]$ yields numerical results up to the machine limit accuracy. Therefore, the DSC algorithm is practically robust for scientific computing.

Second, we test the controllability of the accuracy of the DSC algorithm by changing M. Several M values are used, and r is optimized for each M as shown in Figure 4. Again, the numerical results agree well with the dispersive error analysis. The machine accuracy is reached when $M = 60$ for this problem. Therefore, the DSC algorithm can provide controllable accuracy by varying the parameter M. As a consequence, one of the advantage of the DSC algorithm is its robustness and allows the selection of desirable accuracy for a given problem without any need to change one's computer code.

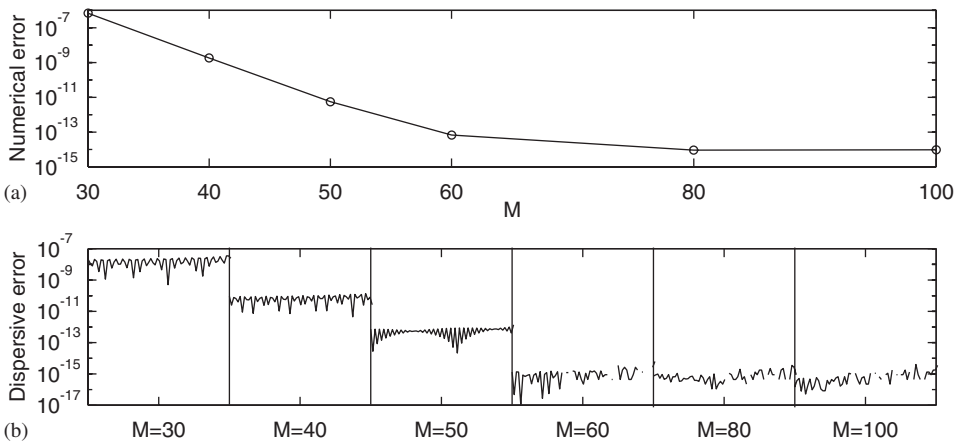

Figure 4. Discretization errors with different M values: (a) the numerically tested H^1-seminorm relative errors; and (b) the dispersive error of the DSC algorithm with $M = 30, 40, 50, 60, 80$ and 100, within $0 \leqslant \omega \leqslant 2.07$.

4.2. Pollution effect test of the DSC algorithm

In this subsection, we numerically investigate the pollution effect of the DSC algorithm. Conventionally, to verify the presence of the pollution effect, the dependence of the relative convergent rate between the FE solution and the corresponding best approximation on the wavenumber k should be tested [3, 9, 14]. However, because the DSC algorithm has a different mathematical foundation from the FE method, it is relatively difficult to identify the best approximation for a particular DSC discretization. Thus, the conventional testing procedure of the pollution effect [3, 9, 14] is inapplicable to the DSC algorithm. In the present study, the presence of the pollution effect may be verified by increasing k under the constraint that kh is a constant. If the numerical error does not evidently increase or even decrease, as k increases, such an algorithm can be regarded as a pollution-free method.

We first test the approximation errors of the DSC algorithm with fixed bandwidth $M = 100$. In Figure 5, the relative error of the DSC solution in the H^1-seminorm is plotted for different k. It is clear that the DSC approximation can achieve extremely high accuracy by using a relatively low grid density for high wavenumbers. Intuitively, the fixed bandwidth might be interpreted as the fixed numerical truncation (polynomial) order. However, it has been proved that the truncation error of the DSC algorithm decays exponentially with respect to the increase in sampling points [25]. This exponential decay can also be clearly observed in Figure 5. Furthermore, it can be seen from Figure 5 that the lines with $kh = \text{constant}$ are almost flat, even though the error slowly increases along these lines. This suggests that the pollution effect of the DSC algorithm with fixed bandwidth is negligible, due to the spectral resolution of the DSC algorithm.

Since the accuracy of the DSC algorithm can be controlled by changing M, as the wavenumber k increases, a larger bandwidth M is required. We thus consider the previous problem by varying M and employing correspondingly optimized r. Figure 6 clearly indicates that the error significantly decreases along the lines $kh = \text{constant}$. Therefore, the DSC algorithm can be essentially free of pollution error for the one-dimensional Helmholtz equation with high wavenumbers.

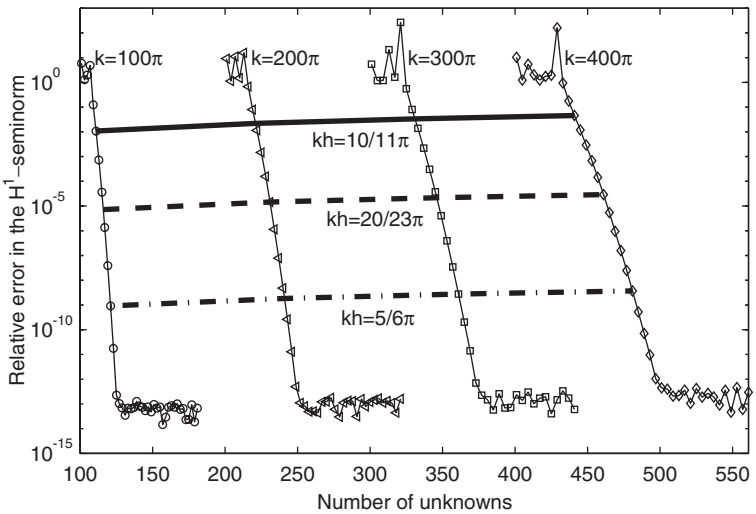

Figure 5. Pollution error of the DSC solutions for a one-dimensional model problem. Four high wavenumbers are considered, i.e. $k = 100\pi,\ 200\pi,\ 300\pi$ and 400π. For all wavenumbers, the DSC parameters are fixed as $M = 100$ and $r = 13$.

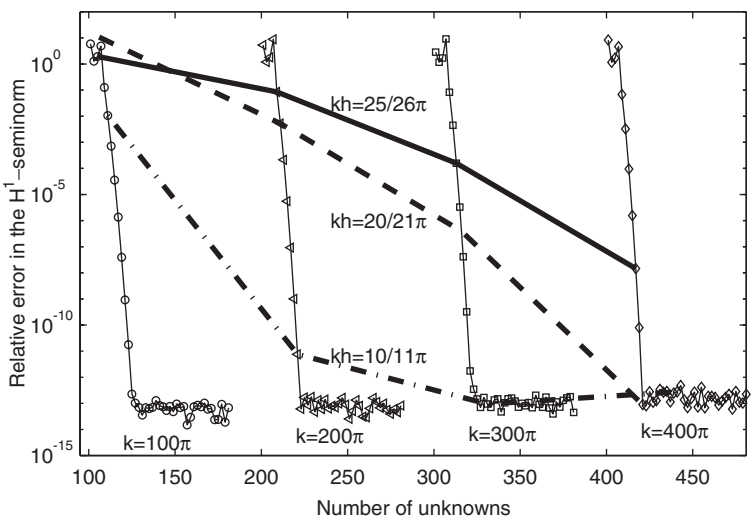

Figure 6. Pollution error testing of the DSC solutions for a one-dimensional model problem. The model problem and tested wavenumbers are the same as in Figure 5. For $k = 100\pi,\ 200\pi,\ 300\pi$ and 400π, the DSC parameters are chosen as $(M, r) = (100, 13),\ (200, 26.2),\ (300, 39.2)$ and $(400, 53.0)$, respectively.

4.3. The Helmholtz equation in higher dimensions

Babuška and Sauter [3] have shown that it is possible to design a stable FE method which is free of pollution error for the one-dimensional Helmholtz equation with high wavenumbers. However, for two- and higher-dimensional cases, the pollution error of the FE solution cannot

be eliminated completely. Therefore, in order to demonstrate the DSC algorithm as a practical pollution-free scheme, it is essential to study the multi-dimensional models. A two-dimensional BVP of the Helmholtz equation is studied for this purpose [9]

$$-\Delta u - k^2 u = 0, \quad \text{in } \Omega = (0,1) \times (0,1) \tag{38}$$

with boundary conditions

$$\mathrm{i}ku + \frac{\partial u}{\partial n} = g, \quad \text{on } \Gamma := \partial\Omega \tag{39}$$

where the symbol $\partial/\partial n$ stands for the outward normal derivative. Here the function g depends on the wave direction angle θ and is given by

$$g(\mathbf{x}) := \begin{cases} \mathrm{i}(k-k_2)\mathrm{e}^{\mathrm{i}k_1 x_1} & \text{if } \mathbf{x} \in \Gamma_1 := (0,1) \times (0,0) \\ \mathrm{i}(k+k_1)\mathrm{e}^{\mathrm{i}(k_1+k_2 x_2)} & \text{if } \mathbf{x} \in \Gamma_2 := (1,1) \times (0,1) \\ \mathrm{i}(k+k_2)\mathrm{e}^{\mathrm{i}(k_1 x_1+k_2)} & \text{if } \mathbf{x} \in \Gamma_3 := (0,1) \times (1,1) \\ \mathrm{i}(k-k_1)\mathrm{e}^{\mathrm{i}k_2 x_2} & \text{if } \mathbf{x} \in \Gamma_4 := (0,0) \times (0,1) \end{cases} \tag{40}$$

with $(k_1, k_2) = k(\cos\theta, \sin\theta)$. The exact solution of this model problem is

$$u(\mathbf{x}) = \mathrm{e}^{\mathrm{i}(k_1 x_1 + k_2 x_2)} \tag{41}$$

Note that this problem has rotational symmetry with respect to $\theta = \pi/4$ [9], and k_j is the wavenumber in the x_j direction for $j = 1, 2$.

It is well known that for the multi-dimensional Helmholtz equation, the approximation error of the FE solutions depends significantly on the wave direction θ [9, 16]. Thus, we first test the change of the approximation errors of the DSC algorithm by using different wave directions θ. Again, the perfect boundary modelling by using the exact solution is employed. For fixed N, M, and r, three k values are tested, the resulting errors are depicted in Figure 7. It is easily seen that results are also rotationally symmetric, except for values that reach the double precision limit. The minimal numerical error is usually achieved at $\theta = \pi/4$.

Generally speaking, if no additional error is introduced by the numerical scheme even when the wave direction is neither on x_1 nor x_2 direction, then the final numerical error of a two-dimensional wave computation should be the larger one of the approximation errors occurred in the single x_1 or x_2 direction. In other words, for such a numerical scheme, the properties of one-dimensional approximation could be directly generalized to multi-dimensional cases. In the present study, the exact rotational symmetry of both the problem and the numerical solution suggests that the DSC algorithm does not induce additional numerical errors for higher-dimensional cases other than that for the one-dimensional one. The reason of the virtual dependence of θ shown in Figure 7 is that different θ implies different values of wavenumbers on the x_1 and x_2 directions, when k is fixed. In fact, the quality of the DSC approximation for the two-dimensional problem depends on $\max(k_1, k_2)$, instead of k or θ. This may be confirmed by noting that the minimal numerical error appears at $\theta = \pi/4$, where $\max(k_1, k_2)$ takes the minimum. To further illustrate this observation, four points in Figure 7 are connected, i.e. $(k, \theta) = (96, 0)$, $(k, \theta) = (64\sqrt{3}, \pi/6)$, $(k, \theta) = (64\sqrt{3}, \pi/3)$, and $(k, \theta) = (96, \pi/2)$. These

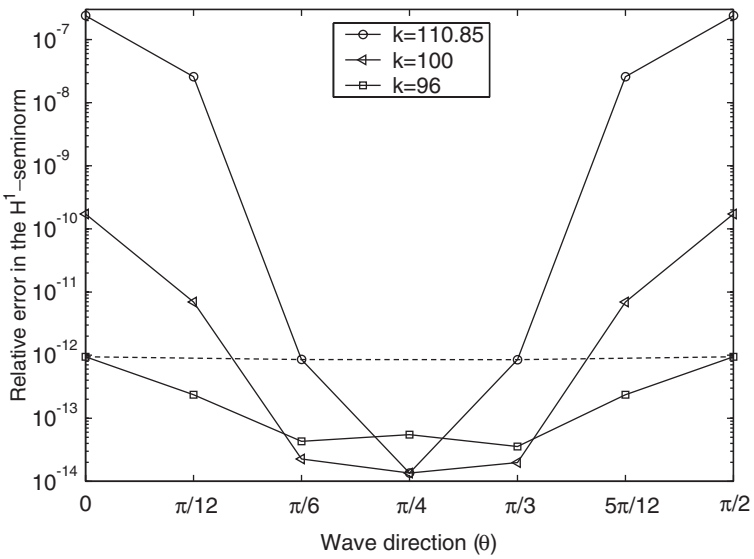

Figure 7. Dependence of the DSC approximation error on the angle θ. Here $N = 51$, $M = 50$ and $r = 6.3$. Three k values are tested: $k = 64\sqrt{3}$, 100 and 96.

four points have the same value of $\max(k_1, k_2)$ and it is clear from graph that the numerical errors of these points are almost the same. Therefore, the numerical characteristic of the DSC algorithm for one-dimensional problems also holds for higher-dimensional cases.

We next numerically test the pollution effect of the DSC algorithm for the multi-dimensional Helmholtz equation with high wavenumbers. Similar to the previous cases, several k values are selected, uniform meshes of size $N \times N$ for different N are used. Following Babuška and Sauter [3], the maximal numerical error among a set of θ values is reported

$$e_1^{\max} := \max_{\theta \in \Theta} e_1(\theta) \tag{42}$$

where $\Theta = \{0, \pi/16, \pi/8, 3\pi/16, \pi/4, 3\pi/8\}$. Figure 8 shows the maximal H^1 errors of a series of numerical experiments. It is obvious that the error decays significantly along the lines $kh = \text{constant}$. Therefore, the DSC algorithm is also free of pollution error for the multi-dimensional Helmholtz equation involving high wavenumbers. It is noted that this conclusion is consistent with the previous discussions.

4.4. Large scale problems

Large scale problems are of special interest to computational electromagnetics, for instance, the computation of the radar cross section for an entire airplane. Initial modelling of such problems often leads to the Helmholtz equation. For a small or moderate scale problem of the Helmholtz equation, to obtain a reasonable accuracy, more than 10 elements per wavelength are typically required by using the FE methods [7, 8, 16]. The situation could get even worse for the large scale problems, due to the pollution effect. Therefore, large scale problems are computationally intractable for many existing numerical methods, such as the standard finite difference or FE methods.

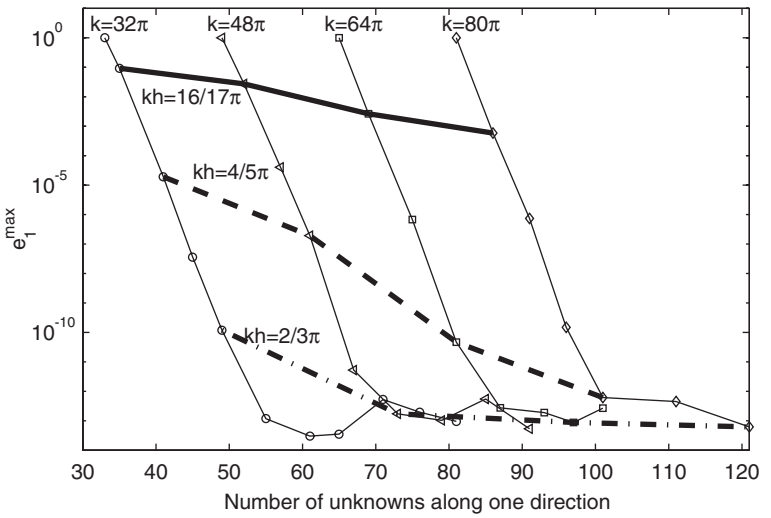

Figure 8. Pollution error of the DSC solution for a two-dimensional model problem. Four k values are tested: $k = 32\pi,\ 48\pi,\ 64\pi$ and 80π. The DSC bandwidth is chosen as $M = N - 1$ at which r is optimized.

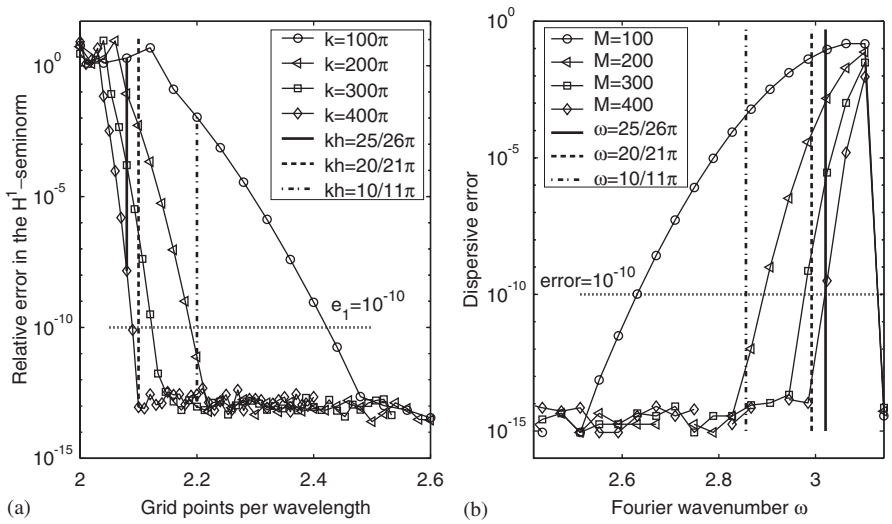

Figure 9. Plots of one-dimensional results and dispersion analysis: (a) plots of relative error in the H^1-seminorm against PPW; and (b) corresponding dispersion analysis.

In the present study, it is of great interest to explore the potential of the DSC algorithm for solving large scale problems since the DSC algorithm has been shown to be essentially pollution free. To this end, the DSC results shown in Figure 6 are re-plotted against the PPW Figure 9(a). The corresponding dispersive errors of the DSC approximation are also shown in Figure 9(b). Again, it can be easily observed that the same pattern appears in both the

Table I. Number of grid points per wavelength needed for the accuracy of 1.0×10^{-10} in the H^1-seminorm.

k	100π	200π	300π	400π
PPW	2.42	2.19	2.12	2.09

Table II. The numerical errors of the DSC algorithm for large scale problems of the one-dimensional Helmholtz equation.

k	N	M	r	PPW	e_1
1250π	1291	1290	80.0	2.064	2.65×10^{-13}
2500π	2571	2570	90.4	2.056	5.68×10^{-13}
5000π	5126	5125	99.9	2.05	8.99×10^{-12}
10000π	10251	10250	98.7	2.05	5.83×10^{-11}

numerical results and the dispersion analysis. It is noted that since $kh = \text{constant}$ implies the identical level of resolution, the lines with $kh = \text{constant}$ become vertical in both graphs. As shown in Figure 9(b), along these vertical lines, as the wavenumber k increases, a larger M can be used to reduce the dispersive error. Consequently, the numerical error is also smaller in Figure 9(a). A more in-depth understanding may be gained if one considers horizontal lines on the graphs, instead of vertical lines. If 1.0×10^{-10} is the acceptable accuracy level, it is clear from Figure 9(b) that when M is larger, the DSC algorithm can provide satisfactory results over larger wavenumber range. In other words, the minimum grid density required to achieve $e_1 = 1.0 \times 10^{-10}$ approaches 2 PPW, as confirmed in the numerical studies, see Figure 9(a) and Table I. In fact, when $M \to \infty$, the grid density requirement for achieving the machine limit accuracy tends to 2 PPW, i.e. the Nyquist frequency. Therefore, the DSC algorithm is well suited for large scale problems, due to the significant savings of the memory and CPU time.

We finally consider several large scale computation problems which are usually intractable by using the conventional finite difference and FE methods. The one-dimensional BVP (35) is employed for this purpose and the wavenumber k as high as 10000π is considered, see Table II. From the table, it is clear that extremely accurate results may be obtained by using a low grid density for these challenging problems.

5. CONCLUSION

This paper investigates the pollution effect and explores the utility of a local spectral method, the discrete singular convolution (DSC) algorithm for solving the Helmholtz equation with high wavenumbers. By means of discrete Fourier analysis, the DSC algorithm is shown to be a dispersion vanishing scheme. The connection between the dispersive error analysis and its practical impact is established via numerical experiments. Both one-and higher-dimensional model problems are employed to numerically demonstrate that the DSC algorithm is essentially free of the pollution error for solving the Helmholtz equation. Large scale problems are also studied to explore the ability of the DSC algorithm for accurate computations with the grid density very close to 2 PPW, i.e. the Nyquist sampling rate limit.

The Fourier analysis indicates that the dispersive error of the DSC algorithm decays as M increases. For fixed M, the dispersive error can be optimized by an appropriate choice of r.

These observations are confirmed by numerical studies. Based on the discrete Fourier analysis, a simple yet general method is suggested to choose an optimal r for a fixed M. The robustness of this method of selection is discussed and demonstrated. Finally, by using a large M, the dispersive error of the DSC algorithm is shown to be vanishing.

In the present paper, the pollution effect of the DSC algorithm for the Helmholtz equation with high wavenumbers is investigated. It is well known that the pollution error is directly related to the dispersion error [2, 8, 10, 13]. As a dispersion vanishing scheme, the pollution error of the DSC algorithm with a fixed bandwidth M is found to be negligible for the one-dimensional model problem. Furthermore, when k is large, a larger M may be chosen for the DSC algorithm so that the numerical error of the DSC solution decreases rapidly along the lines $kh = \text{constant}$. Therefore, the DSC algorithm is essentially free of the pollution error for the one-dimensional Helmholtz equation.

The pollution error of the DSC algorithm for the multi-dimensional Helmholtz equation is also considered. In the multi-dimensions case, the pollution effect of the finite element methods is known to be inevitable in principle [3]. As a collocation method, the implementation of the DSC algorithm for multi-dimensions is essentially the same as in a one-dimensional case. Thus, the numerical properties of the DSC algorithm for one-dimensional studies generally remain valid for the multi-dimensional case, as demonstrated in our numerical experiments. Therefore, the DSC algorithm is also free of the pollution error in multi-dimensions.

As an essentially pollution-free scheme, the feasibility of the DSC algorithm for large scale computations in wave propagation is explored. Our present study shows that the spectral accuracy may be achieved in the DSC solutions by employing a sampling rate that is close to the optimal Nyquist sampling rate for large scale computations.

In summary, the work indicates that the DSC algorithm is accurate and efficient for solving the Helmholtz equation with high wavenumbers.

ACKNOWLEDGEMENTS

This work was supported in part by the National University of Singapore and Michigan State University. The work of Gang Bao was supported partially by the NSF Applied Mathematics Programs grant DMS 01-04001 and the Office of Naval Research grant N000140210365. He also wishes to thank the Mathematics Department of the City University of Hong Kong for its hospitality and support during the course of this work.

REFERENCES

1. Ihlenburg F, Babuška I. Finite element solution of the Helmholtz equation with high wavenumber part I: the h-version of the FEM. *Computers and Mathematics with Applications* 1995; **30**:9–37.
2. Ihlenburg F, Babuška I. Finite element solution of the Helmholtz equation with high wavenumber part II: the h-p-version of the FEM. *SIAM Journal on Numerical Analysis* 1997; **34**:315–358.
3. Babuška I, Sauter SA. Is the pollution effect of the FEM avoidable for the Helmholtz equation considering high wave number? *SIAM Journal on Numerical Analysis* 1997; **34**:2392–2423. Reprinted in *SIAM Review* 2000; **42**:451–484.
4. Giladi E, Keller JB. A hybrid numerical asymptotic method for scattering problems. *Journal of Computational Physics* 2001; **174**:226–247.
5. Zienkiewicz OC. Achievements and some unsolved problems of the finite element method. *International Journal for Numerical Methods in Engineering* 2000; **47**:9–28.
6. Dautray R, Lions L. *Mathematical Analysis and Numerical Methods for Science and Technology*, vol. I. Springer: New York, 1990.
7. Harari I, Hughes TJR. Finite element methods for the Helmholtz equation in an exterior domain: model problems. *Computer Methods in Applied Mechanics and Engineering* 1991; **87**:59–96.

8. Babuška I, Ihlenburg F, Strouboulis T, Gangaraj SK. A posteriori error estimation for finite element solutions of Helmholtz equation. Part I: the quality of local indicators and estimators. *International Journal for Numerical Methods in Engineering* 1997; **40**:3443–3462.
9. Babuška I, Ihlenburg F, Paik ET, Sauter SA. A generalized finite element method for solving the Helmholtz equation in two dimensions with minimal pollution. *Computer Methods in Applied Mechanics and Engineering* 1995; **128**:325–359.
10. Ihlenburg F, Babuška I. Dispersion analysis and error estimation of Galerkin finite element methods for the Helmholtz equation. *International Journal for Numerical Methods in Engineering* 1995; **38**:3745–3774.
11. Babuška I, Strouboulis T, Upadhyay CS, Gangaraj SK. A posteriori estimation and adaptive control of the pollution error in the *h*-version of the finite element method. *International Journal for Numerical Methods in Engineering* 1995; **38**:4207–4235.
12. Babuška I, Ihlenburg F, Strouboulis T, Gangaraj SK. A posteriori error estimation for finite element solutions of Helmholtz equation. Part II: estimation of the pollution error. *International Journal for Numerical Methods in Engineering* 1997; **40**:3883–3900.
13. Deraemaeker A, Babuška I, Bouillard P. Dispersion and pollution of the FEM solution for the Helmholtz equation in one, two and three dimensions. *International Journal for Numerical Methods in Engineering* 1999; **46**:471–499.
14. Gerdes K, Ihlenburg F. On the pollution effect in FE solutions of the 3D-Helmholtz equation. *Computer Methods in Applied Mechanics and Engineering* 1999; **170**:155–172.
15. Vichnevetsky R, Bowles JB. *Fourier Analysis of Numerical Approximations of Hyperbolic Equations*. SIAM: Philadelphia, 1982.
16. Thompson LL, Pinsky PM. A Galerkin least-square finite element method for the two-dimensional Helmholtz equation. *International Journal for Numerical Methods in Engineering* 1995; **38**:371–397.
17. Babuška I, Melenk JM. The partition of unity method. *International Journal for Numerical Methods in Engineering* 1997; **40**:727–758.
18. Laghrouche O, Bettess P. Short wave modelling using special finite elements. *Journal of Computational Acoustics* 2000; **8**:189–210.
19. Suleau S, Deraemaeker A, Bouillard P. Dispersion and pollution of meshless solutions for the Helmholtz equation. *Computer Methods in Applied Mechanics and Engineering* 2000; **190**:639–657.
20. Farhat C, Harari I, Franca LP. The discontinuous enrichment method. *Computer Methods in Applied Mechanics and Engineering* 2001; **190**:6455–6479.
21. Laghrouche O, Bettess P, Astley RJ. Modelling of short wave diffraction problem using approximating systems of plane waves. *International Journal for Numerical Methods in Engineering* 2002; **54**:1501–1533.
22. Wei GW. Discrete singular convolution for the solution of the Fokker–Planck equation. *Journal of Chemical Physics* 1999; **110**:8930–8942.
23. Wei GW. Wavelets generated by using discrete singular convolution kernels. *Journal of Physics A—Mathematical and General* 2000; **33**:8577–8596.
24. Wei GW. A unified approach for the solution of the Fokker–Planck equation. *Journal of Physics A—Mathematical and General* 2000; **33**:4935–4953.
25. Bao G, Wei GW, Zhou AH. Analysis of regularized Whittaker–Kotel'nikov–Shannon sampling expansion, preprint.
26. Wei GW, Zhao YB, Xiang Y. Discrete singular convolution and its application to the analysis of plates with internal supports. I Theory and algorithm. *International Journal for Numerical Methods in Engineering* 2002; **55**:913–946.
27. Xiang Y, Zhao YB, Wei GW. Discrete singular convolution and its application to the analysis of plates with internal supports. II Complex supports. *International Journal for Numerical Methods in Engineering* 2002; **55**:947–971.
28. Zhou YC, Patnaik BSV, Wan DC, Wei GW. DSC solution for flow in a staggered double lid driven cavity. *International Journal for Numerical Methods in Engineering* 2003; **57**:211–234.
29. Thompson LL, Pinsky PM. Complex wavenumber Fourier analysis of the *p*-version finite element method. *Computational Mechanics* 1994; **13**:255–275.
30. Hackbusch W. *Elliptic Differential Equations*. Springer: Berlin, 1992.
31. Givoli D. *Numerical Methods for Problems in Infinite Domains*. Elsevier: Amsterdam/New York, 1992.
32. Wei GW. A new algorithm for solving some mechanical problems. *Computer Methods in Applied Mechanics and Engineering* 2001; **190**:2017–2030.

